

Homogenizing Interfacial Stress by Nanoporous Metal Current Collector to Enable Stable All-Solid-State Li Metal Battery

Shijie Feng,¹ Ram Hemanth Yeerella,¹ Jianbin Zhou, Nimrod Harpak, Chenghai Li, Shengqiang Cai,* and Ping Liu*

Cite This: *ACS Energy Lett.* 2024, 9, 748–757

Read Online

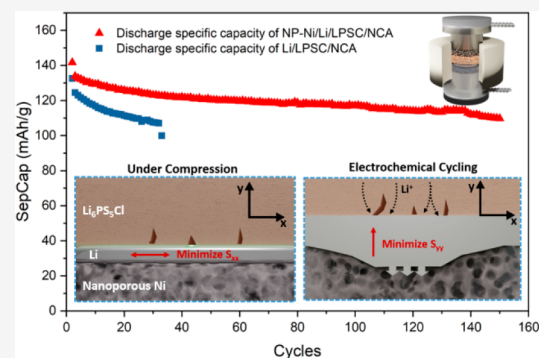
ACCESS |

Metrics & More

Article Recommendations

Supporting Information

ABSTRACT: All-solid-state lithium–metal batteries are prone to shorting due to lithium penetration through the electrolyte layer. Li experiences a creep during compression, inducing stress in the electrolyte layer. Uneven plating and stripping of Li further exaggerate the heterogeneity of the stress distribution. To overcome this challenge, we designed a nanoporous nickel (NP-Ni) current collector. Its textured surface resists Li metal lateral creep, while its compliant nature reduces stress concentration from uneven Li deposition. These mechanisms prevent additional defects in the solid electrolyte layer, mitigating Li penetration during the processes of fabrication and cycling. Experimental observation and finite element modeling validate NP-Ni's ability to homogenize stress distribution. Compared to Ni foil, NP-Ni effectively enhances the critical current density (1.7 vs 0.4 mA/cm²) and extends cycle life (>360 vs 12 h) for Li/Li symmetric cells. The ability of NP-Ni to homogenize the interfacial stress provides a chemistry-agnostic approach to improving the cycle life of solid-state Li batteries.



All-solid-state lithium metal batteries (ASSLMBs) are being widely investigated due to their possible integration in applications such as electric vehicles, portable devices, and grid storage.^{1,2} In comparison to their traditional lithium-ion counterparts, the combination of thermally stable solid-state electrolyte (SSE) and Li metal anode promises a safer system with higher energy density.^{3,4} Research efforts in recent years have brought significant progress, including SSEs that exhibit high ionic conductivities,^{5,6} as well as electrode development and device integration that have yielded promising performances in terms of energy density and cycle life. For example, an “anode free” battery based on the Li₆PS₄Cl (LPSC) electrolyte demonstrated an energy density surpassing 900 Wh L⁻¹, along with a remarkable longevity of over 1000 cycles.⁷ The battery employed a Ag–C interlayer, which was crucial in regulating Li deposition.

Despite promising progress, substantial challenges persist in the field of ASSLMBs.⁸ Both chemical and mechanical instabilities are well documented. In order to maintain intimate contact between different solid component materials and layers,⁹ solid state batteries are fabricated under extreme pressures (>350 MPa)¹⁰ and are usually operated under significant pressure as well (>30 MPa), although progress has been made to lower them.^{11,12} High operating pressures are

required to mitigate the effects of the volumetric change of electrodes during cycling. Poor interfacial stability between Li metal and the electrolyte is also well-known. Li metal exhibits irreversible chemical and electrochemical reactions^{13–16} and the concomitant impedance rise, capacity loss, and even shorting events,¹⁷ especially when operating under high current densities.

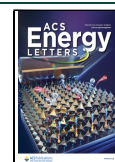
Shorting of solid-state batteries has been a persistent challenge under a variety of pressurization conditions.^{17,18} Many studies have identified uncontrollable Li dendrite growth as the primary cause for cell failure.^{19,20} When utilizing inorganic SSEs, nonuniform Li growth generates local stress, leading to spallation and cracks in the SSE layer, subsequently allowing Li penetration and causing cell shorting.^{21–23} The formation and propagation of Li dendrites can be attributed to various factors, including the discontinuous interfacial contact

Received: December 11, 2023

Revised: January 22, 2024

Accepted: January 26, 2024

Published: January 31, 2024



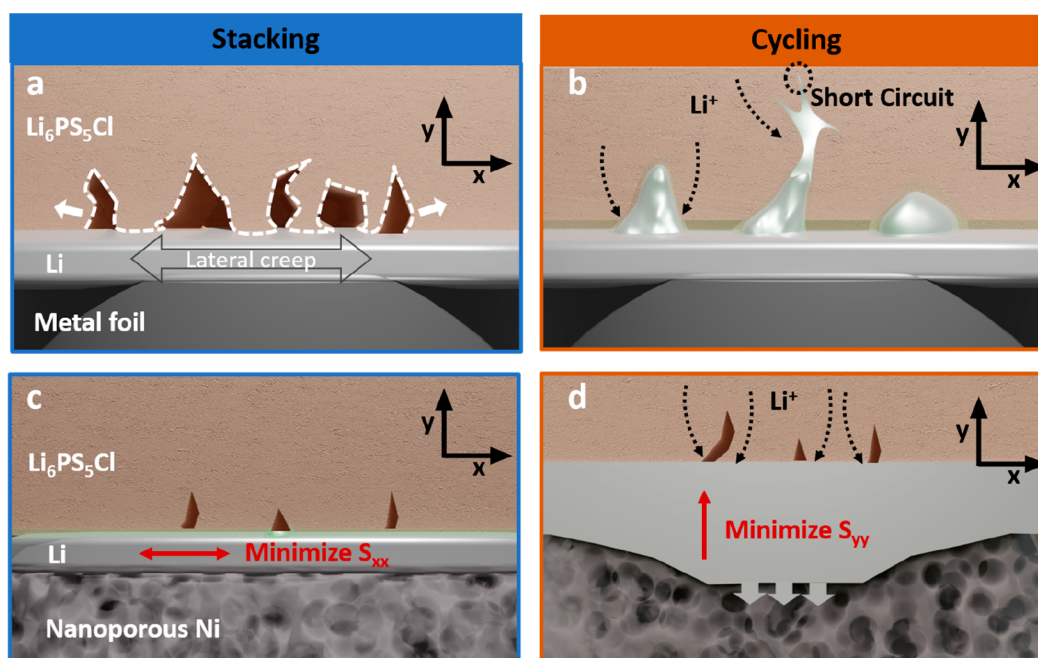


Figure 1. Schematic illustrations of (a) surface crack formation due to the stress generated by Li metal lateral creep deformation during stacking. (b) Li dendrite formation due to the nonuniform interface during electrochemical cycling. (c) Textured surface of the NP-Ni current collector minimizes normal stress in horizontal direction on solid electrolyte surface. (d) Low mechanical modulus of the NP-Ni current collector minimizes normal stress in the vertical direction on a solid electrolyte surface.

between Li and SSE, the presence of a grain boundary within the SSE and the electronic conductivity of SSE that assists in inducing dendrites. From a contact perspective, the discontinuous interface between Li and SSE results in significant interfacial resistance and irregular distribution of Li ion flux.²⁴ Additionally, higher local ionic resistivity and lower shear modulus of the grain boundary, compared to the bulk, promote the Li dendrite formation.^{25–27} Moreover, SSEs that possess relatively high electronic conductivities enable lithium ions to combine with electrons, forming dendrites inside pores of the SSE.²⁸ Therefore, mechanical failure induced by dendrites within the electrolyte layer consistently begins with the onset of inhomogeneity. Once a crack emerges due to local stress, lithium will ingress into the crack and traverse through the SSE layer, resulting in internal shorting.²²

Various solutions have been proposed to address these failure mechanisms. From the perspective of SSEs, single crystalline or grain-boundary-free structures aim to fundamentally eliminate the effects of defects inherent in polycrystalline materials.²⁹ Additionally, focusing on the interface, a silver (Ag)/lithium fluoride (LiF) bilayer structure has been introduced. In this setup, the Ag layer serves as a lithophilic interlayer that facilitates physical contact through alloying with lithium metal, while the LiF layer acts as an electrophobic interlayer, preventing electrical leakage due to non-negligible electronic conductivities and effectively suppressing dendrite growth.³⁰ Similar functionality has also been observed with a poly(acrylic acid) (LiPPA) interlayer.³¹ Alternative anode designs have also been explored to replace traditional Li metal. For instance, a Li/graphite paste has been developed due to its low viscosity and enhanced wettability with garnet-type SSE.³² Moreover, 3D porous anode structures, such as nickel foam, have been introduced to accommodate local volume changes during the plating and stripping cycles. These structures have

been found to help in suppressing Li dendrite growth during electrochemical cycling.^{33–35}

To further study the shorting behavior of ASSLMs, it is important to deconvolute the effect of mechanical compression and electrochemical cycling. As specified, maintaining a solid–solid contact requires immense fabrication pressures and high operating pressures. Bulk Li metal exhibits low yield strength, ranging from 0.4–1.2 MPa,^{36,37} and therefore is bound to experience creep deformation which is expected to transmit mechanical stress to the surrounding SSE layer. This results in a nonuniform contact and even cracking of the SSE, which even happens before electrochemical cycling takes place. Due to the poor compatibility between Li and the electrolyte layer, subsequent deposition and stripping of Li are often inhomogeneous. This leads to a further increase in uneven stress distribution and formation of voids and cracks. As a consequence, addressing both the pure mechanically driven and electrochemically driven shorting events is essential to the realization of a stable ASSLM.

Herein, we introduce a free-standing nanoporous nickel (NP-Ni) current collector designed for the Li metal anode, showcasing a stress-minimization effect at the interface of Li and the LPSC. This stress minimization is achieved through the frictional force between Li and NP-Ni, coupled with the elastic compliance capability of NP-Ni. The NP-Ni current collector has enabled an average critical current density (CCD) of 1.7 mA/cm² and exhibited over 360 h of cycling life in Li/Li symmetric cells, a significant improvement over a metal foil control. Furthermore, ASSLM with a LiNi_{0.85}Co_{0.1}Al_{0.05}O₂ (NCA) cathode and NP-Ni anode current collector demonstrated over 150 cycles of stable cycling, retaining 83% of its original capacity. Our approach offers a promising strategy to mechanically stabilize the interface between Li metal and LPSC, thereby achieving a stable ASSLM.

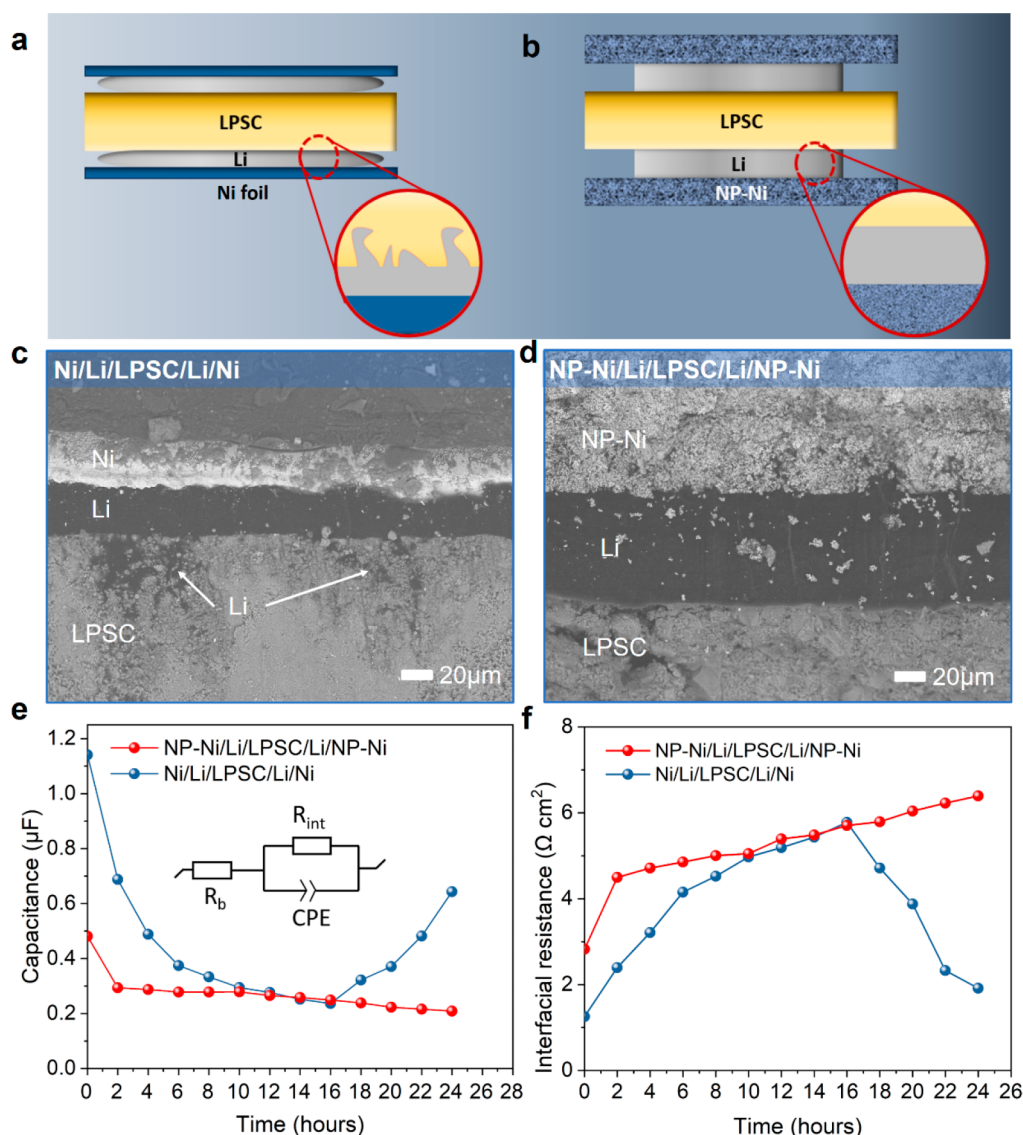


Figure 2. (a, b) Schematic configurations of Li/Li symmetric cells with/without NP-Ni, where the perfect interface was generated using NP-Ni after compression. (c, d) Cross-section SEM images of the Li/LPSC electrolyte interface after 30 MPa compression with/without the NP-Ni current collector, respectively. (e) Calculated capacitance of two symmetric cells along with the time under 30 MPa compression. (f) Evolution of interfacial resistance between Li and LPSC extracted from EIS.

DESIGN AND FABRICATION OF THE NANOPOROUS NICKEL CURRENT COLLECTOR

The porous nickel current collector is designed to have the ability to minimize the stress on the surface of the LPSC during both mechanical compression and electrochemical cycling. Due to the significant stack pressure applied, inevitable lateral creeping of Li leads to the formation of large defects on the LPSC surface which promotes Li penetration (Figure 1a). Subsequent nonuniform Li growth during electrochemical cycling exacerbates dendrite formation and causes short circuit (Figure 1b). When the porous Ni current collector is applied, the frictional force provided by its textured surface resists Li metal lateral creep and minimizes the tensile stress in the horizontal direction (S_{xx}) during the cell fabrication process (Figure 1c). The vertical local stress (S_{yy}) arising during Li stripping and plating can also be homogenized due to the high compliance of the porous Ni current collector underneath (Figure 1d). Stress minimization helps to prevent the LPSC from fracturing and being penetrated by Li.

To achieve the aforementioned functions of the current collector, finite element analysis (FEM) was utilized to uncover the specific properties of porous Ni. Preventing the entrapment of Li metal in the pores of the current collector during mechanical compression is essential. This issue can impede further utilization of the filled Li and compromise the stress-adapting function of the current collector. Thus, investigations were conducted on Li behavior on porous Ni with various sizes of pores under mechanical compression (Figure S1). A circular hole was assumed on the surface of the Ni layer with three different radii (50 μm , 20 μm , 10 μm). The Li layer was placed between the LPSC and the Ni layer, replicating the actual cell configuration. Based on FEM simulation results, with 8 MPa uniaxial compression, it was observed that pores with a 10 μm radius had the least Li entrapment (Figure S1a). In the case of 20- μm radius pores, however, Li was observed to cave into the pores, leading to relatively nonuniform normal stress along the vertical direction (Figure S1b). Full filling was observed in the 50 μm case,

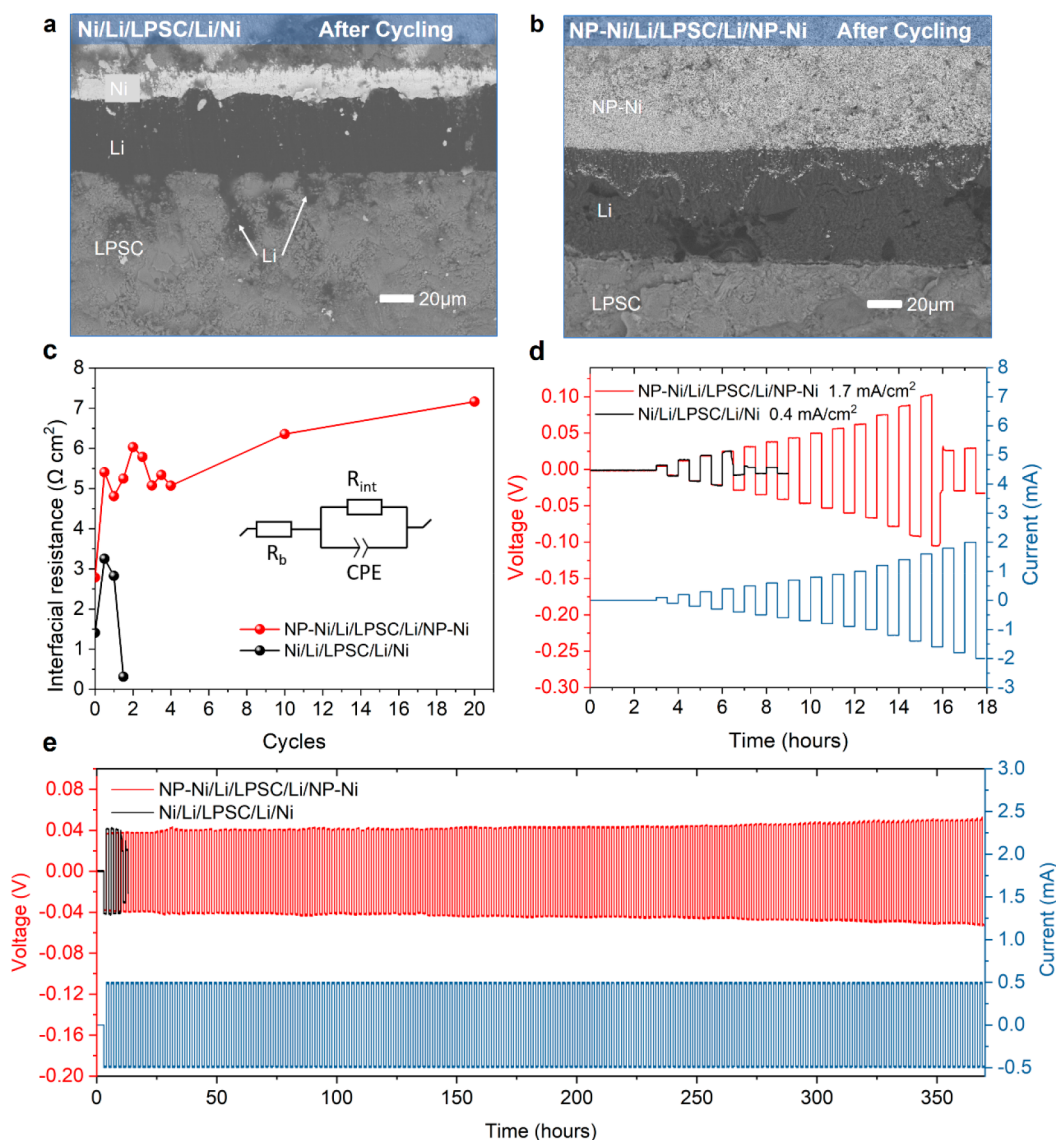


Figure 3. (a, b) Cross-section SEM images of Li/LPSC electrolyte interface after cycling at 0.5 mA/cm² with/without NP-Ni, respectively; (c) evolution of Interfacial resistance between Li and LPSC in NP-Ni/Li/LPSC/Li/NP-Ni and Li/LPSC/Li cells during cycling. (d) Critical current density comparison; (e) long-term cycling performance comparison under a 0.5 mA/cm² current density and 0.5 mAh capacity.

causing an even higher stress inhomogeneity in the electrolyte layer (Figure S1c). Consequently, Ni with smaller pores demonstrates a more favorable function during mechanical compression. To accommodate the actual stacking pressure of 30 MPa, Ni with pores and ligaments hundreds of nanometer in size was selected, which is termed nanoporous nickel (NP-Ni).

The described physical properties of the NP-Ni are realized via the use of nanoporous Ni powder as the precursor, which is, in turn, synthesized by hydrogen reduction of Ni salts. By using different precursors and a controlled annealing process to the intermediate, NP-Ni with ligaments and pores on the order of hundreds of nanometers can be synthesized (Figure S2a).^{38,39} Detailed synthesis information is provided in the experimental section in the Supporting Information. Powder X-ray diffraction (XRD) (Figure S2b) confirmed a pure Ni phase, which indicates the reduction reaction was complete. An ~200 μm thick, free-standing NP-Ni current collector is fabricated via cold pressing of the nanoporous powder. Figure S2c, d indicates that mechanical compression does not affect

the morphology of NP-Ni. A 100 μm thick Li foil was then pressed onto the NP-Ni current collector at a pressure of 30 MPa. No Li metal was observed inside the submicrometer pores of the NP-Ni current collector (Figure S3), which confirmed the FEM modeling results.

■ EFFECT OF NP-NI ON LI CREEP UNDER UNIAXIAL COMPRESSION

To investigate the benefits of using an NP-Ni current collector, a Li/Li symmetric cell was assembled. The cell contains an LPSC pellet that is ~800 μm thick and ~1.3 cm² in size sandwiched by two pieces of Li metal that are 100 μm thick and ~0.7 cm² in size. An NP-Ni current collector of ~1.3 cm² in size is attached to the Li on each side. The cell is denoted as NP-Ni/Li/LPSC/Li/NP-Ni. A Ni/Li/LPSC/Li/Ni cell with bulk Ni foil was also assembled as a control (Figure 2a,).

Cold-pressed LPSC pellets generally exhibit defects and pores on the surface (Figure S4).⁴⁰ During cell assembly, lithium metal is compressed along with the LPSC pellet at a

pressure of 30 MPa. Noticeable Li penetration into the pores of the LPSC layer is observed in the cross-sectional images of cells with the Ni foil current collector, using the backscattering mode of a scanning electron microscope (SEM) (Figure 2c). The presence of the NP-Ni current collector, in contrast, helps maintain a uniform and intimate interface between the Li metal and the LPSC (Figure 2d). Interfacial images from multiple regions are provided in Figure S5 and in the Supporting Information. This lack of Li penetration is mainly attributed to the frictional force applied on the Li that limits the lateral creep and the tensile force applied to the LPSC by the laterally expanding Li. When the pressure reaches 30 MPa, the Li metal thickness is noticeably decreased from $\sim 100\ \mu\text{m}$ to $\sim 35\ \mu\text{m}$ with the Ni foil current collector. With the NP-Ni, however, the change is reduced from $\sim 100\ \mu\text{m}$ to $\sim 73\ \mu\text{m}$. Less deformation results in less lateral stress that was applied to the defects and pores on the LPSC surface. To better visualize the dimensional change of Li, $\sim 0.44\ \text{cm}^2$ round Li metal chips were sandwiched between transparent plastic sheets and two current collectors. After compressing at 30 MPa, Li metal underwent an $\sim 56\%$ area expansion ($0.44\ \text{cm}^2$ to $0.69\ \text{cm}^2$) with an $\sim 29\%$ thickness reduction with the Ni foil current collector (Figure S6a, b), while only an $\sim 19\%$ area expansion ($0.44\ \text{cm}^2$ to $0.52\ \text{cm}^2$) along with an $\sim 6\%$ thickness reduction was observed with the NP-Ni current collector (Figure S6c, d). The friction coefficient (μ) between Li metal and the current collector surface was also measured by a plane sliding method under constant speed.⁴¹ According to the following equation:

$$\mu = \frac{F_f}{F_n} \quad (1)$$

Where F_f is the measured friction force and F_n is the measured normal force, the interface between NP-Ni and Li displays a measured μ of 0.768, while the corresponding value for the Ni foil current collector is 0.329 (Figure S7a). This difference in the friction coefficient is consistent with our observation of the Li creep behavior under compression. Hence, the rough surface of the NP-Ni current collector shows a better capability to resist lateral deformation, which is expected to reduce the horizontal stress exerted by Li to the surface of the electrolyte layer and minimize additional mechanical damage.

We next use electrochemical impedance spectroscopy (EIS) to quantify the evolution of the Li/electrolyte interface upon compression applied during the cell fabrication process (Figure S8).⁴² The capacitance⁴³ and interfacial resistance can be extracted from the EIS data by fitting with the equivalent circuit shown in Figure 2e and used as measures for the quality and stability of the Li/LPSC interface. After 16 h of compression under 30 MPa, the capacitance value started to increase (Figure 2e) in the case of the Ni foil current collector, which indicates an increase in the contact area between Li and LPSC, likely due to Li penetration.⁴⁴ At the same time, a decrease of the interfacial resistance was also observed (Figure 2f), which also indicates Li metal penetration into the LPSC layer.⁴⁵ However, with the NP-Ni current collector, the interfacial resistance and capacitance are relatively stable after 24 h (Figure 2e, f). The slight increase of the resistance ($4.4\ \Omega\ \text{cm}^2$ to $6.4\ \Omega\ \text{cm}^2$) is attributed to the interphases generated by the spontaneous reaction between Li and LPSC.⁴⁶

EFFECT OF NP-NI ON THE EVOLUTION OF THE LI/LPSC INTERFACE DURING THE ELECTROCHEMICAL PROCESS

The Li/Li symmetric cells with both current collectors are then cycled at a current density of $0.5\ \text{mA}/\text{cm}^2$ and capacity of $0.5\ \text{mAh}/\text{cm}^2$. SEM images of the device cross sections are shown in Figures 3a,b. After a few cycles, Li metal penetration into the electrolyte layer is clearly observed with the Ni foil current collector (Figure 3a). Li penetration during cell assembly appears to have led to nonuniform Li^+ flux, which promotes uneven Li deposition and local stress accumulation, eventually leading to further Li penetration and cell failure. In contrast, the NP-Ni current collector serves as a compliant mechanical buffer at the back side of Li metal which homogenizes the interfacial stress and releases local stresses concentration generated by uneven Li deposition.⁴⁵ As a result, an intimate dendrite-free interface can be obtained after 180 cycles (Figure 3b). EIS analysis was also applied to monitor the interface evolution during the cycling of the two symmetric cells. Resistance drop was observed for the Ni foil current collector cell after the first cycle. The cell shorted soon after. In contrast, the interfacial resistance is maintained at $\sim 6\ \Omega\ \text{cm}^2$ stably in the cell using the NP-Ni current collector (Figure 3c). The capacitance also remains stable after 20 cycles (Figure S9). Both cross-sectional SEM images and EIS results demonstrate that adding an NP-Ni current collector helps to maintain a stable Li/LPSC interface. As a result, the NP-Ni/Li/LPSC/Li/NP-Ni symmetric cell demonstrated an average critical current density (CCD) of $1.7\ \text{mA}/\text{cm}^2$ (Figure 3d), more than 4 times higher than that of the Li/LPSC/Li cell with foil current collectors ($0.4\ \text{mA}/\text{cm}^2$). CCD, defined as the current density at which a short circuit occurs, is a commonly used metric to characterize the cells' resistance to shorting.⁴⁷ Multiple tests were conducted for both cells (Figure S10) in order to prevent stochastic variability. Further, the use of the NP-Ni current collector also enables the symmetric cell to cycle for over 360 h at room temperature at a current density of $0.5\ \text{mA}/\text{cm}^2$, while the control cell only lasts for less than 10 h (Figure 3e).

The effect of stress homogenization during cycling was further investigated using a one-way deposition method. Li was electrochemically deposited to one side at $0.1\ \text{mA}/\text{cm}^2$ in both types of symmetric cells until cell failure (Figure S11a). Analysis of the voltage curve revealed that the NP-Ni/Li/LPSC/Li/NP-Ni cell was able to deposit approximately $8\ \text{mAh}/\text{cm}^2$ of Li ($\sim 40\ \mu\text{m}$) to the other side without displaying any signs of interface failure. In contrast, the control cell showed a stable movement of only about $3\ \text{mAh}/\text{cm}^2$ of Li ($\sim 15\ \mu\text{m}$), as indicated by voltage fluctuations. This confirms that the inclusion of NP-Ni contributes to improving the quality of the interface during Li plating and stripping processes.

Following the one-way electrodeposition, no Li metal was observed inside the porous structure of NP-Ni (Figure S11b, c). Additionally, after long-term cycling, no overlapping signals from O (a surrogate for Li presence) and Ni through energy dispersive spectroscopy (EDS) elemental mapping confirm that Li metal did not cave into pores of NP-Ni (Figure S12). Hence, it is established that lithium does not infiltrate the pores in both the mechanical and electrochemical processes. Accommodating local stress generated by lithium is not achieved by the extra room provided by the pores of NP-Ni, which aligns with the intended design.

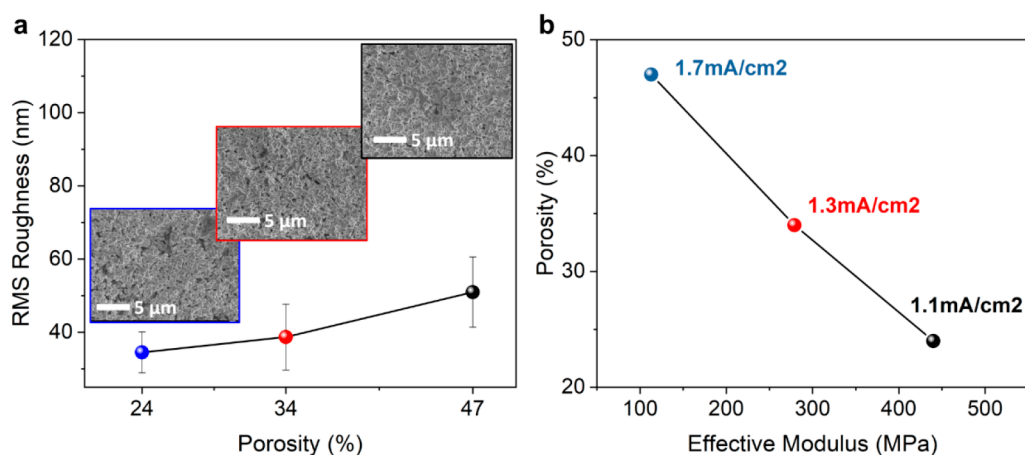


Figure 4. (a) RMS roughness difference of NP-Ni current collectors with various porosity. SEM images of the corresponding surface of NP-Ni current collectors are shown inside. (b) The inverse relationship between the effective modulus of NP-Ni and the critical current density of corresponding symmetric cells.

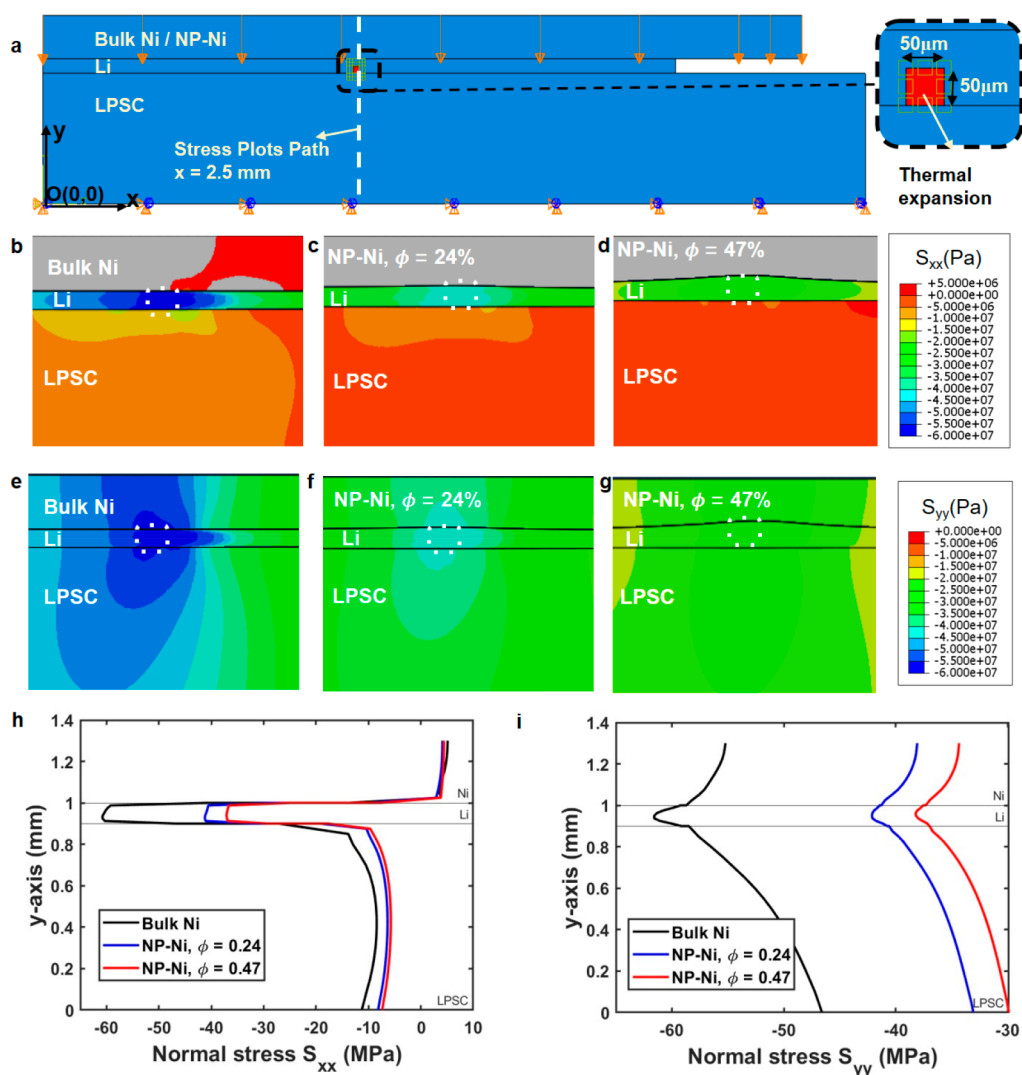


Figure 5. Finite element simulation results. (a) ABAQUS model depiction. (b–d) Distribution of normal stress in the horizontal direction for different types of Current collectors. (e–g) Distribution of normal stress in the vertical direction for the different types of current collectors. (h) Normal stress in the horizontal direction (S_{xx}) plotted along the described path. (i) Normal stress in the vertical direction (S_{yy}) plotted along the described path.

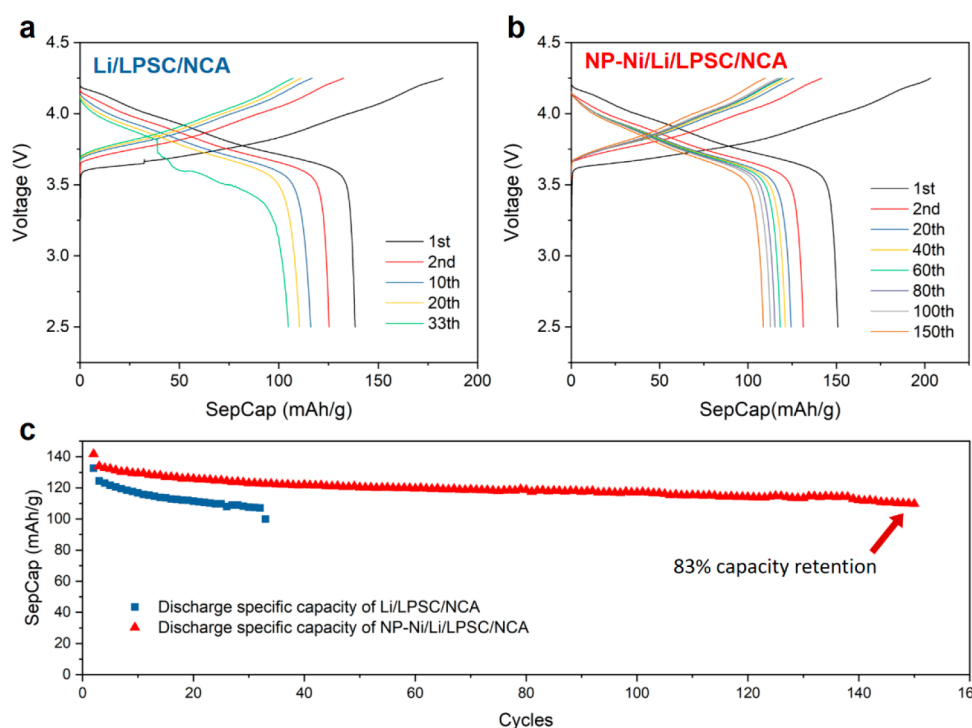


Figure 6. Electrochemical cycling performance of solid-state Li metal-NCA full cells. (a, b) Charge and discharge profiles of Li/LPSC/NCA and NP-Ni/Li/LPSC/NCA, respectively. (c) Corresponding discharge capacity of two cells.

■ QUANTIFYING THE NP-NI OPERATING MECHANISM

We hypothesized that the unique mechanical property of the NP-Ni current collector helps to accommodate local stress generated during the electrochemical process. To examine this hypothesis, three NP-Ni current collectors were fabricated with different porosities and moduli. Similar surface morphologies were obtained (Figure 4a). Atomic force microscopy (AFM) revealed that the difference of their RMS roughness is less than 15 nm (Figure 4a, S13), which will result in similar friction coefficients^{48,49} as well as similar creeping behavior of Li during the cell fabrication process. By employing three NP-Ni current collectors, we can investigate the influence of mechanical compliance of NP-Ni during the electrochemical process.

Nanoindentation was employed to measure the compliance of the three NP-Ni current collectors. The local deformation during the nanoindentation can be used to imitate stress accumulation during Li dendrite growth. The effective indentation moduli of 133, 279, and 440 MPa were obtained for NP-Ni with porosities of $\sim 47\%$, $\sim 34\%$, and $\sim 24\%$ (Figure S14a), respectively. We note these values are on the same order of magnitude as the growth stress of Li dendrites.⁵⁰ CCD results were obtained from symmetric cells with the three NP-Ni samples (Figure S14b-S14d) are all significantly improved over the foil control (0.4 mA/cm^2), yet an inverse correlation was also observed between the modulus and CCD (Figure 4b), which revealed that NP-Ni with relatively higher compliance results in a better cell performance. Therefore, it is evident that the softer NP-Ni can provide better stress accommodation during the electrochemical cycling.

These experimental observations were substantiated through a 3-step Finite Element simulation. The model is built as shown in Figure 5a, with bulk Ni/NP-Ni as the top layer, Li in

the middle, and LPSC at the bottom. A simple elastoplastic model is used to describe the material behavior of these layers. We first compress the stack in Step 1 up to a certain load, and in Step 2 we wait until there is no significant change in the deformation field. The results of these two processes help us to understand the stress profile in the cell during assembly. In Step 3, we introduce an isotropic thermal expansion to a small area in Li, marked in red color within the dotted box as shown in Figure 5a, to mimic uneven Li deposition or Li dendrite growth. All of the modeling parameters are itemized in Tables S1 and S2. We observed that the stresses generated in the Bulk Ni/NP-Ni layer and LPSC layer are well within their elastic limits, essentially making them behave like linear elastic materials (Figure S15), for the current loading conditions. Only Li would undergo plastic deformation.

The application of a NP-Ni current collector enables stress homogenization. Despite being subjected to equivalent compression pressures, the deployment of NP-Ni has yielded a more evenly distributed stress profile (Figure S16b, S16c), leading to a discernible reduction in peak stress along both horizontal and vertical directions. The Li metal is susceptible to sliding and consequent creep deformation after sustained compression over a duration. This phenomenon induces stress relaxation, albeit at the risk of introducing defects. Employing NP-Ni, characterized by its rougher surface, preserves its stress state with diminished relaxation tendencies. This substantiates the potential for mitigating Li lateral creep and protecting the LPSC surface during mechanical compacting, which is consistent with the experimental results.

The presented contour plots within Figure 5b - 5g elucidate the normal stress distribution after localized volumetric expansion caused by Li uneven deposition. Figure 5b - 5d and Figure 5e - 5g represent the normal stress in the horizontal direction and the vertical direction, respectively. The deformation is scaled by a factor of 2, to help better visualize

the local compression in the NP-Ni layer. Compared with the bulk Ni current collector (Figure 5b, 5e), the utilization of NP-Ni as the current collector allows notable deformation within the NP-Ni layer itself, thereby effectively reducing the magnitude of localized stresses resulting from volumetric expansion (Figure 5c, 5f). We observe a greater deformation in the NP-Ni layer and a reduction in the stress localization through NP-Ni with a lower effective modulus (Figure 5d, 5g). It demonstrates that high compliance of NP-Ni helps to accommodate the local volume expansion and promote battery stability (Figure S16d, S16e). Figures 5h and 5i illustrate the stress distributions along a vertical path through the thermal expansion region, where peak stresses manifest. Incorporating an NP-Ni current collector reduced the peak compressive stress by over 20 MPa in both the horizontal and vertical directions. Reduced stress magnitudes are also observed with the use of a more compliant NP-Ni current collector. Therefore, the rough surface and compliant properties of the NP-Ni current collector help to uniformize stress distribution and minimize normal stress in the x and y directions on the surface of LPSC. The former can reduce the probability of forming significant defects, while the latter directly reduces the chance of Li penetration, which brings about an enhancement of the battery stability.

DEMONSTRATION OF PERFORMANCE ENHANCEMENT IN SOLID STATE BATTERIES

The NP-Ni current collector is then implemented in solid-state Li metal batteries with a $\text{LiNi}_{0.85}\text{Co}_{0.1}\text{Al}_{0.05}\text{O}_2$ (NCA) cathode. Cathode composite is composed of 66 wt % NCA, 33 wt % LPSC and 1 wt % VGCF and the capacity loading is 1.6 mAh cm^{-2} . 0.1 mA/ cm^2 current density was applied during the first formation cycle, followed by 0.3 mA/ cm^2 for subsequent cycles. The coulombic efficiency (CE) of the initial cycle is 71% for Li/LPSC/NCA and 74% for NP-Ni/Li/LPSC/NCA. These observed efficiencies are consistent with values reported in prior studies.^{10,51,52} Nevertheless, employing NCA with an advanced coating has the potential to further improve these values. In terms of the cycling performance, the Li/LPSC/NCA cell (Figure 6a) experienced quick capacity degradation and failed after 33 cycles, while the NP-Ni/Li/LPSC/NCA cell (Figure 6b) demonstrated a stable cycling performance with 83% capacity retention after 150 cycles (Figure 6c). Additional full cell data are provided in Figure S17 which also depicted a comparable result. In addition, Li metal – NCA full cells with a 5 MPa stacking pressure were assembled to demonstrate the effectiveness of our strategy in low-pressure battery applications. The NP-Ni cell exhibited a higher CE (74% compared to 67% for the control) in the first cycle (Figure S18), which is attributable to the homogeneous interface facilitated by NP-Ni. These significant improvements, achieved with identical electrode and electrolyte chemistry, demonstrate the potential of using NP-Ni to mitigate the stress generation and provide a chemistry agnostic solution to a difficult stability problem of solid-state batteries.

By designing a nanoporous nickel current collector with hundreds of nanometer-sized pores and ligaments and implementing it in solid-state Li metal batteries, we have demonstrated that interfacial stress can be accommodated and homogenized, which enhances battery long-term stability. The friction provided by the rough surface of NP-Ni resists Li metal lateral creep, resulting in the minimization of horizontal stress on the surface of the LPSC electrolyte. Additionally, the high

mechanical compliance of NP-Ni helps to mitigate the local stress concentration caused by uneven Li deposition. Validated by finite element simulation, both effects protect the LPSC electrolyte, preventing the creation of more defects during compression and Li stripping and plating. Enhanced critical current density (CCD) (1.7 mA/ cm^2) and cycling life (>360 h) at 0.5 mA/ cm^2 are achieved in Li/Li symmetric cells. A remarkable improvement is also observed in Li/NCA full cells, with 83% capacity retention after 150 cycles, a 5× improvement over the control cell. Our design provides a chemistry-agnostic approach to extending the cycle life of solid-state Li-metal batteries.

ASSOCIATED CONTENT

Supporting Information

The Supporting Information is available free of charge at <https://pubs.acs.org/doi/10.1021/acsenergylett.3c02681>.

Experimental details, finite element simulation details, NP-Ni morphology characterization, LPSC pellet morphology, Li lateral creep measurement after compression, coefficient of friction measurement, electrochemical impedance spectroscopy data, one-way stripping data, energy dispersive spectroscopy data, atomic force microscopy data, CCD vs NP-Ni with different moduli, modeling parameter tables (PDF)

AUTHOR INFORMATION

Corresponding Authors

Shengqiang Cai – Department of Mechanical and Aerospace Engineering, University of California San Diego, La Jolla, California 92093, United States; orcid.org/0000-0002-6852-7680; Email: shqcai@ucsd.edu

Ping Liu – Materials Science and Engineering Program, University of California San Diego, La Jolla, California 92093, United States; Department of Nanoengineering, University of California San Diego, La Jolla, California 92093, United States; orcid.org/0000-0002-1488-1668; Email: piliu@ucsd.edu

Authors

Shijie Feng – Materials Science and Engineering Program, University of California San Diego, La Jolla, California 92093, United States; orcid.org/0000-0001-5797-8542

Ram Hemanth Yeerella – Department of Mechanical and Aerospace Engineering, University of California San Diego, La Jolla, California 92093, United States; orcid.org/0000-0002-9344-6313

Jianbin Zhou – Department of Nanoengineering, University of California San Diego, La Jolla, California 92093, United States

Nimrod Harpak – Department of Nanoengineering, University of California San Diego, La Jolla, California 92093, United States

Chenghai Li – Department of Mechanical and Aerospace Engineering, University of California San Diego, La Jolla, California 92093, United States

Complete contact information is available at:

<https://pubs.acs.org/doi/10.1021/acsenergylett.3c02681>

Author Contributions

[†]S.F. and H.Y. contributed equally to this paper.

Notes

The authors declare no competing financial interest.

ACKNOWLEDGMENTS

This work has been supported by the Advanced Research Projects Agency-Energy, U.S. Department of Energy, under Contract No. DE-AR0000781. Part of this work was performed at the San Diego Nanotechnology infrastructure (SDNI) of the UCSD, a member of the National Nanotechnology Coordinated infrastructure, supported by the National Science Foundation (Grant ECCS-1542148).

REFERENCES

- (1) Albertus, P.; Anandan, V.; Ban, C.; Balsara, N.; Belharouak, I.; Buettner-Garrett, J.; Chen, Z.; Daniel, C.; Doeff, M.; Dudney, N. J.; Dunn, B.; Harris, S. J.; Herle, S.; Herbert, E.; Kalnaus, S.; Libera, J. A.; Lu, D.; Martin, S.; McCloskey, B. D.; McDowell, M. T.; Meng, Y. S.; Nanda, J.; Sakamoto, J.; Self, E. C.; Tepavcevic, S.; Wachsman, E.; Wang, C.; Westover, A. S.; Xiao, J.; Yersak, T. Challenges for and Pathways toward Li-Metal-Based All-Solid-State Batteries. *ACS Energy Letters* **2021**, *1399–1404*.
- (2) Wu, D.; Wu, F. Toward better batteries: Solid-state battery roadmap 2035+. *eTransportation* **2023**, *16*, 100224.
- (3) Meabe, L.; Aldalur, I.; Lindberg, S.; Arrese-Igor, M.; Armand, M.; Martinez-Ibañez, M.; Zhang, H. Solid-state electrolytes for safe rechargeable lithium metal batteries: a strategic view. *Materials Futures* **2023**, *2*, 033501.
- (4) Yu, X.; Chen, R.; Gan, L.; Li, H.; Chen, L. Battery Safety: From Lithium-Ion to Solid-State Batteries. *Engineering* **2023**, *21*, 9–14.
- (5) Janek, J.; Zeier, W. G. Challenges in speeding up solid-state battery development. *Nature Energy* **2023**, *8* (3), 230–240.
- (6) Li, X.; Liang, J.; Yang, X.; Adair, K. R.; Wang, C.; Zhao, F.; Sun, X. Progress and perspectives on halide lithium conductors for all-solid-state lithium batteries. *Energy Environ. Sci.* **2020**, *13* (5), 1429–1461.
- (7) Lee, Y.-G.; Fujiki, S.; Jung, C.; Suzuki, N.; Yashiro, N.; Omoda, R.; Ko, D.-S.; Shiratsuchi, T.; Sugimoto, T.; Ryu, S.; Ku, J. H.; Watanabe, T.; Park, Y.; Aihara, Y.; Im, D.; Han, I. T. High-energy long-cycling all-solid-state lithium metal batteries enabled by silver-carbon composite anodes. *Nature Energy* **2020**, *5* (4), 299–308.
- (8) Wang, J.; Chen, L.; Li, H.; Wu, F. Anode Interfacial Issues in Solid-State Li Batteries: Mechanistic Understanding and Mitigating Strategies. *Energy Environ. Mater.* **2023**, *6* (4), e12613.
- (9) Zhao, K.; Cui, Y. Understanding the role of mechanics in energy materials: A perspective. *Extreme Mechanics Letters* **2016**, *9*, 347–352.
- (10) Doux, J.-M.; Yang, Y.; Tan, D. H. S.; Nguyen, H.; Wu, E. A.; Wang, X.; Banerjee, A.; Meng, Y. S. Pressure effects on sulfide electrolytes for all solid-state batteries. *Journal of Materials Chemistry A* **2020**, *8* (10), 5049–5055.
- (11) Sang, J.; Tang, B.; Qiu, Y.; Fang, Y.; Pan, K.; Zhou, Z. How Does Stacking Pressure Affect the Performance of Solid Electrolytes and All-Solid-State Lithium Metal Batteries? *Energy Environ. Mater.* **2023**, e12670.
- (12) Hänsel, C.; Kundu, D. The Stack Pressure Dilemma in Sulfide Electrolyte Based Li Metal Solid-State Batteries: A Case Study with $\text{Li}_3\text{PS}_4\text{Cl}$ Solid Electrolyte. *Adv. Mater. Interfaces* **2021**, *8* (10), 2100206.
- (13) Paul, P. P.; Chen, B.-R.; Langevin, S. A.; Dufek, E. J.; Nelson Weker, J.; Ko, J. S. Interfaces in all solid state Li-metal batteries: A review on instabilities, stabilization strategies, and scalability. *Energy Storage Materials* **2022**, *45*, 969–1001.
- (14) Byeon, Y.-W.; Kim, H. Review on Interface and Interphase Issues in Sulfide Solid-State Electrolytes for All-Solid-State Li-Metal Batteries. *Electrochem* **2021**, *2* (3), 452–471.
- (15) Pang, Y.; Pan, J.; Yang, J.; Zheng, S.; Wang, C. Electrolyte/Electrode Interfaces in All-Solid-State Lithium Batteries: A Review. *Electrochemical Energy Reviews* **2021**, *4* (2), 169–193.
- (16) Shen, X.; Zhang, R.; Chen, X.; Cheng, X. B.; Li, X.; Zhang, Q. The Failure of Solid Electrolyte Interphase on Li Metal Anode: Structural Uniformity or Mechanical Strength? *Adv. Energy Mater.* **2020**, *10* (10), 1903645.
- (17) Ke, X.; Wang, Y.; Dai, L.; Yuan, C. Cell failures of all-solid-state lithium metal batteries with inorganic solid electrolytes: Lithium dendrites. *Energy Storage Materials* **2020**, *33*, 309–328.
- (18) Doux, J.-M.; Nguyen, H.; Tan, D. H. S.; Banerjee, A.; Wang, X.; Wu, E. A.; Jo, C.; Yang, H.; Meng, Y. S. Stack Pressure Considerations for Room-Temperature All-Solid-State Lithium Metal Batteries. *Adv. Energy Mater.* **2020**, *10* (1), 1903253.
- (19) Liu, J.; Yuan, H.; Liu, H.; Zhao, C. Z.; Lu, Y.; Cheng, X. B.; Huang, J. Q.; Zhang, Q. Unlocking the Failure Mechanism of Solid State Lithium Metal Batteries. *Adv. Energy Mater.* **2022**, *12* (4), 2100748.
- (20) Mangani, L. R.; Villevieille, C. Mechanical vs chemical stability of sulphide-based solid-state batteries. Which one is the biggest challenge to tackle? Overview of solid-state batteries and hybrid solid state batteries. *Journal of Materials Chemistry A* **2020**, *8* (20), 10150–10167.
- (21) Gao, H.; Ai, X.; Wang, H.; Li, W.; Wei, P.; Cheng, Y.; Gui, S.; Yang, H.; Yang, Y.; Wang, M. S. Visualizing the failure of solid electrolyte under GPa-level interface stress induced by lithium eruption. *Nat. Commun.* **2022**, *13* (1), 5050.
- (22) Ning, Z.; Jolly, D. S.; Li, G.; De Meyere, R.; Pu, S. D.; Chen, Y.; Kasemchainan, J.; Ihli, J.; Gong, C.; Liu, B.; Melvin, D. L. R.; Bonnin, A.; Magdysyuk, O.; Adamson, P.; Hartley, G. O.; Monroe, C. W.; Marrow, T. J.; Bruce, P. G. Visualizing plating-induced cracking in lithium-anode solid-electrolyte cells. *Nat. Mater.* **2021**, *20* (8), 1121–1129.
- (23) Hatzell, K. B.; Chen, X. C.; Cobb, C. L.; Dasgupta, N. P.; Dixit, M. B.; Marbella, L. E.; McDowell, M. T.; Mukherjee, P. P.; Verma, A.; Viswanathan, V.; Westover, A. S.; Zeier, W. G. Challenges in Lithium Metal Anodes for Solid-State Batteries. *ACS Energy Letters* **2020**, *5* (3), 922–934.
- (24) Cao, D.; Sun, X.; Li, Q.; Natan, A.; Xiang, P.; Zhu, H. Lithium Dendrite in All-Solid-State Batteries: Growth Mechanisms, Suppression Strategies, and Characterizations. *Matter* **2020**, *3* (1), 57–94.
- (25) Yu, S.; Siegel, D. J. Grain Boundary Softening: A Potential Mechanism for Lithium Metal Penetration through Stiff Solid Electrolytes. *ACS Appl. Mater. Interfaces* **2018**, *10* (44), 38151–38158.
- (26) Raj, R.; Wolfenstine, J. Current limit diagrams for dendrite formation in solid-state electrolytes for Li-ion batteries. *J. Power Sources* **2017**, *343*, 119–126.
- (27) Cheng, E. J.; Sharafi, A.; Sakamoto, J. Intergranular Li metal propagation through polycrystalline $\text{Li}_{6.25}\text{Al}_{0.25}\text{La}_3\text{Zr}_2\text{O}_{12}$ ceramic electrolyte. *Electrochim. Acta* **2017**, *223*, 85–91.
- (28) Han, F.; Westover, A. S.; Yue, J.; Fan, X.; Wang, F.; Chi, M.; Leonard, D. N.; Dudney, N. J.; Wang, H.; Wang, C. High electronic conductivity as the origin of lithium dendrite formation within solid electrolytes. *Nature Energy* **2019**, *4* (3), 187–196.
- (29) Sastre, J.; Futscher, M. H.; Pompizi, L.; Aribia, A.; Priebe, A.; Overbeck, J.; Stiefel, M.; Tiwari, A. N.; Romanyuk, Y. E. Blocking lithium dendrite growth in solid-state batteries with an ultrathin amorphous Li-La-Zr-O solid electrolyte. *Communications Materials* **2021**, *2* (1), 76.
- (30) Lee, S.; Lee, K.-s.; Kim, S.; Yoon, K.; Han, S.; Lee, M. H.; Ko, Y.; Noh, J. H.; Kim, W.; Kang, K. Design of a lithiophilic and electron-blocking interlayer for dendrite-free lithium-metal solid-state batteries. *Science Advances* **2022**, *8* (30), eabq0153.
- (31) Huo, H.; Gao, J.; Zhao, N.; Zhang, D.; Holmes, N. G.; Li, X.; Sun, Y.; Fu, J.; Li, R.; Guo, X.; Sun, X. A flexible electron-blocking interfacial shield for dendrite-free solid lithium metal batteries. *Nat. Commun.* **2021**, *12* (1), 176.
- (32) Duan, J.; Wu, W.; Nolan, A. M.; Wang, T.; Wen, J.; Hu, C.; Mo, Y.; Luo, W.; Huang, Y. Lithium-Graphite Paste: An Interface Compatible Anode for Solid-State Batteries. *Adv. Mater.* **2019**, *31* (10), e1807243.

(33) Chi, S.-S.; Liu, Y.; Song, W.-L.; Fan, L.-Z.; Zhang, Q. Prestoring Lithium into Stable 3D Nickel Foam Host as Dendrite-Free Lithium Metal Anode. *Adv. Funct. Mater.* **2017**, *27* (24), 1700348.

(34) Wan, H.; Wang, Z.; Liu, S.; Zhang, B.; He, X.; Zhang, W.; Wang, C. Critical interphase overpotential as a lithium dendrite-suppression criterion for all-solid-state lithium battery design. *Nature Energy* **2023**, *8* (5), 473–481.

(35) Chen, Y.; Wang, Z.; Li, X.; Yao, X.; Wang, C.; Li, Y.; Xue, W.; Yu, D.; Kim, S. Y.; Yang, F.; Kushima, A.; Zhang, G.; Huang, H.; Wu, N.; Mai, Y. W.; Goodenough, J. B.; Li, J. Li metal deposition and stripping in a solid-state battery via Coble creep. *Nature* **2020**, *578* (7794), 251–255.

(36) Fincher, C. D.; Ojeda, D.; Zhang, Y.; Pharr, G. M.; Pharr, M. Mechanical properties of metallic lithium: from nano to bulk scales. *Acta Mater.* **2020**, *186*, 215–222.

(37) Masias, A.; Felten, N.; Garcia-Mendez, R.; Wolfenstine, J.; Sakamoto, J. Elastic, plastic, and creep mechanical properties of lithium metal. *J. Mater. Sci.* **2019**, *54* (3), 2585–2600.

(38) Lu, L.; Andela, P.; De Hosson, J. T. M.; Pei, Y. Template-Free Synthesis of Nanoporous Nickel and Alloys as Binder-Free Current Collectors of Li Ion Batteries. *ACS Appl. Nano Mater.* **2018**, *1* (5), 2206–2218.

(39) Feng, S.; Petrova, V.; Corrao, A. A.; Wang, S.; Yang, K.; Khalifah, P. G.; Liu, P. Morphological Control of Nanoporous Copper Formed from Conversion Reaction Synthesis. *J. Phys. Chem. C* **2022**, *126* (35), 14878–14885.

(40) Sakuda, A.; Hayashi, A.; Tatsumisago, M. Sulfide solid electrolyte with favorable mechanical property for all-solid-state lithium battery. *Sci. Rep.* **2013**, *3*, 2261.

(41) Gratton, L. M.; DeFrancesco, S. A simple measurement of the sliding friction coefficient. *Phys. Educ.* **2006**, *41* (3), 232–235.

(42) Lee, C.; Han, S. Y.; Lewis, J. A.; Shetty, P. P.; Yeh, D.; Liu, Y.; Klein, E.; Lee, H.-W.; McDowell, M. T. Stack Pressure Measurements to Probe the Evolution of the Lithium-Solid-State Electrolyte Interface. *ACS Energy Letters* **2021**, *6* (9), 3261–3269.

(43) Chang, B.-Y. The Effective Capacitance of a Constant Phase Element with Resistors in Series. *Journal of Electrochemical Science and Technology* **2022**, *13* (4), 479–485.

(44) Liu, P.; Vajo, J. J.; Wang, J. S.; Li, W.; Liu, J. Thermodynamics and Kinetics of the Li/FeF₃ Reaction by Electrochemical Analysis. *J. Phys. Chem. C* **2012**, *116* (10), 6467–6473.

(45) Zhang, X.; Xiang, Q.; Tang, S.; Wang, A.; Liu, X.; Luo, J. Long Cycling Life Solid-State Li Metal Batteries with Stress Self-Adapted Li/Garnet Interface. *Nano Lett.* **2020**, *20* (4), 2871–2878.

(46) Schwietert, T. K.; Vasileiadis, A.; Wagemaker, M. First-Principles Prediction of the Electrochemical Stability and Reaction Mechanisms of Solid-State Electrolytes. *JACS Au* **2021**, *1* (9), 1488–1496.

(47) Lu, Y.; Zhao, C.-Z.; Yuan, H.; Cheng, X.-B.; Huang, J.-Q.; Zhang, Q. Critical Current Density in Solid-State Lithium Metal Batteries: Mechanism, Influences, and Strategies. *Adv. Funct. Mater.* **2021**, *31* (18), 2009925.

(48) Zhou, Y.; Zhu, H.; Zhang, W.; Zuo, X.; Li, Y.; Yang, J. Influence of surface roughness on the friction property of textured surface. *Advances in Mechanical Engineering* **2015**, *7* (2), 1687814014568500.

(49) Svahn, F.; Kassman-Rudolph, Å.; Wallén, E. The influence of surface roughness on friction and wear of machine element coatings. *Wear* **2003**, *254* (11), 1092–1098.

(50) Zhang, L.; Yang, T.; Du, C.; Liu, Q.; Tang, Y.; Zhao, J.; Wang, B.; Chen, T.; Sun, Y.; Jia, P.; Li, H.; Geng, L.; Chen, J.; Ye, H.; Wang, Z.; Li, Y.; Sun, H.; Li, X.; Dai, Q.; Tang, Y.; Peng, Q.; Shen, T.; Zhang, S.; Zhu, T.; Huang, J. Lithium whisker growth and stress generation in an in situ atomic force microscope-environmental transmission electron microscope set-up. *Nat. Nanotechnol.* **2020**, *15* (2), 94–98.

(51) Shin, D.; Nam, J. S.; Linh Nguyen, C. T.; Jo, Y.; Lee, K.; Hwang, S. M.; Kim, Y.-J. Design of densified nickel-rich layered composite cathode via the dry-film process for sulfide-based solid-

state batteries. *Journal of Materials Chemistry A* **2022**, *10* (43), 23222–23231.

(52) Banerjee, A.; Tang, H.; Wang, X.; Cheng, J.-H.; Nguyen, H.; Zhang, M.; Tan, D. H. S.; Wynn, T. A.; Wu, E. A.; Doux, J.-M.; Wu, T.; Ma, L.; Sterbinsky, G. E.; D'Souza, M. S.; Ong, S. P.; Meng, Y. S. Revealing Nanoscale Solid-Solid Interfacial Phenomena for Long-Life and High-Energy All-Solid-State Batteries. *ACS Appl. Mater. Interfaces* **2019**, *11* (46), 43138–43145.

Recommended by ACS

Combining Solid Solution Strengthening and Second Phase Strengthening for Thinning Li Metal Foils

Zixing Guo, Wei Luo, *et al.*

JULY 10, 2023

ACS NANO

READ 

Localized Recrystallization of a Lithium-Metal Anode during Fast Stripping in High-Activity Liquid Electrolytes

Shang Zhu, Venkatasubramanian Viswanathan, *et al.*

JANUARY 30, 2023

ACS APPLIED MATERIALS & INTERFACES

READ 

Enhancing Lithium Stripping Efficiency in Anode-Free Solid-State Batteries through Self-Regulated Internal Pressure

Daxian Cao, Hongli Zhu, *et al.*

OCTOBER 11, 2023

NANO LETTERS

READ 

Conformal Coating of a Carbon Film on 3D Hosts toward Stable Lithium Anodes

Zibo Zhang, Zhaoping Liu, *et al.*

JULY 06, 2021

ACS APPLIED ENERGY MATERIALS

READ 

Get More Suggestions >